NANO LETTERS

Letter

pubs.acs.org/NanoLett

Electron Pumping in Graphene Mechanical Resonators

Tony Low,*[,†] Yongjin Jiang,[‡,§] Mikhail Katsnelson,[∥] and Francisco Guinea[⊥]

[†]IBM T.J. Watson Research Center, Yorktown Heights, New York 10598, United States

[‡]Department of Physics, ZheJiang Normal University, Zhejiang 321004, People's Republic of China

[§]Department of Physics, Purdue University, West Lafayette, Indiana 47909, United States

[∥]Institute for Molecules and Materials, Radboud University Nijmegen, Heyendaalseweg 135, 6525AJ Nijmegen, The Netherlands

[⊥]Instituto de Ciencia de Materiales de Madrid, CSIC, Sor Juana Inés de la Cruz 3, 28049 Madrid, Spain

Supporting Information

ABSTRACT: The combination of high-frequency vibrations and metallic transport in graphene makes it a unique material for nanoelectromechanical devices. In this Letter, we show that graphene-based nanoelectromechanical devices are extremely well suited for charge pumping due to the sensitivity of its transport coefficients to perturbations in electrostatic potential and mechanical deformations, with the potential for novel small scale devices with useful applications.

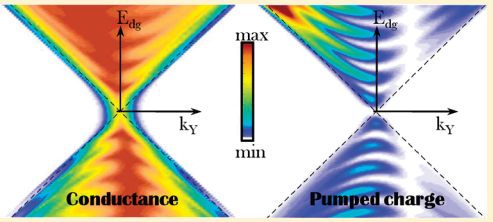

KEYWORDS: *Quantum pumping, suspended graphene, strain, mechanical resonator*

Device miniaturization has led to small-size mechanical systems, nanoelectromechanical (NEMs) devices with a wide range of uses in fundamental and applied research.[1−3] In particular, electron pumps and turnstiles have been extensively studied,[4−6] including NEM-based devices.[7−11] Graphene NEMs[12−14] have an enhanced tunability with respect to devices based on carbon nanotubes, while keeping advantageous features, such as high vibration frequencies and metallicity. Suspended graphene samples have a very high electron mobility[15] and a large and well-characterized electronic coupling to the strains induced by long wavelength vibrations.[16] Long wavelength strains in a ballistic graphene sheet modify the electronic transport coefficients through the sheet.[17] A flexural deformation leads to uniaxial strains within the suspended area, inducing a strain mismatch at the boundary between the suspended and nonsuspended regions, modulating the transport coefficients. Deformations of amplitudes of a few nanometers in samples of micrometers in size and the tuning of its electrostatic doping can be simultaneously achieved by adjusting the electrostatic force between the graphene layer and the metallic gate below it.[17] The periodic modulation in time of these internal parameters, i.e., electrostatic doping and strains, makes it possible to achieve adiabatic charge pumping,[18−20] if the appropriate symmetries are broken. We argue below that these requirements can be met in a realistic experimental setup, leading to charge pumping of the order of a few electrons per cycle.

We analyze the feasibility of a pumping device using the geometry sketched in Figure 1a. The length of the sheet is L, and the applied voltage is $V(t) = V_{dc} + V_{ac}\cos(\omega t)$. We describe the deformation in terms of a single degree of freedom, the maximum vertical displacement, $a(t)$. Its dynamics is determined by the sum of the time-dependent electrostatic force between the sheet and the gate, $\mathcal{F}_E$, the restoring elastic force, $\mathcal{F}_S$, and a dissipative term introduced phenomenologically, $\mathcal{F}_D$:[21]

$$\rho\frac{\partial^2 a}{\partial t^2} = \mathcal{F}_S + \mathcal{F}_D + \mathcal{F}_E$$

$$\mathcal{F}_E = \frac{C_T^2 V_{dc} V_{ac}}{\varepsilon_0}\cos(\omega t)$$

$$\mathcal{F}_S = -\frac{64}{3}\frac{\lambda+2\mu}{L^4}(a^3 + 3a^2 h_0 + 3a h_0^2) + \frac{8\Delta L}{L^3}(\lambda+2\mu)a$$

$$\mathcal{F}_D = -\frac{\rho}{\tau_d}\frac{\partial a}{\partial t} \quad (1)$$

where ρ is the mass density, λ and μ are Lamé elastic constants, C_T is the total effective capacitance due to the back-gate oxide and air dielectric, and ΔL and h_0 describe the amount of slack and vertical displacement of the sheet in the absence of the periodic driving potential. The phenomenological parameter τ_d describes damping, and the quality factor is $Q = (\omega_0\tau_d)/2$, where ω_0 is the resonant frequency. Currently, experimentally obtained ω_0 for graphene is in the range of 100 MHz.[13,14,22] Figure 1b reproduces a typical experimental ω_0 as function of V_{dc} with our model. In the linear response regime, $\omega_0 \approx h_0/L^2\rho^{1/2}$, whereas h_0 can be tuned through V_{dc} and is proportional

Received: November 5, 2011
Revised: January 19, 2012
Published: January 24, 2012

 © 2012 American Chemical Society dx.doi.org/10.1021/nl2038985 | *Nano Lett.* 2012, 12, 850−854

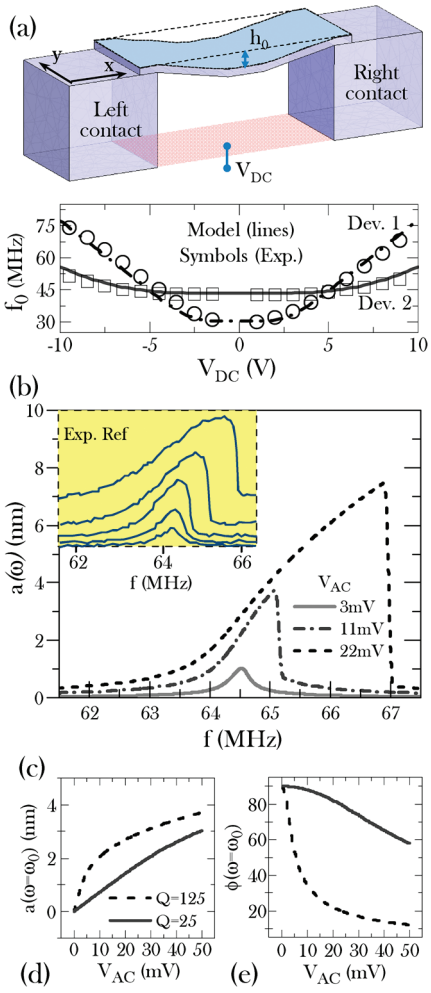

Figure 1. (a) Schematic of a typical graphene nanoelectromechanical resonator actuated electrostatically with a back gate. Gating capacitance is given by the total effective capacitance due to the back-gate oxide and air dielectric, i.e., $C_T = [\varepsilon_0^{-1}(d + h_0) + \varepsilon_{SiO_2}^{-1} t_{SiO_2}]^{-1}$, where we assumed t_{SiO_2} = 200 nm and d = 100 nm in this work. (b) Resonant frequency f_0 as function of bias voltage V_{dc}, computed using our model, i.e., $\omega_0 = (k_0/\rho)^{1/2}$, where $k_0 = \partial_a^2 \mathcal{F}_S(a = 0)$ is the linearized spring constant term. ρ and ΔL are used as fitting parameter to the experimental data of two devices (in symbols) reproduced from ref 14. (c) Amplitude response, $a(\omega)$, of device 1 for different driving forces V_{ac}, obtained by solving the nonlinear resonator model of eq 1 using techniques employed for the Duffing model, assuming a quality factor Q = 125, the value corresponding to the experimental situation.[14] The oscillator shows features of bistability and hysteresis similar to that of experiments[14] (see inset and ref 14 for measurement details). (d–e) Amplitude and phase response at resonance (of device 1) as function of driving force V_{ac} for two different quality factors Q = 25 and 125.

to $(n^2L^4)^{1/3}$. Continual device downscaling and improvements in graphene fabrication processes will allow for GHz operation, already realized in nanotube systems.[23]

We look for the frequency and the phase response to the dynamical system described by eq 1. The equations define a nonlinear resonator, which we solve approximately[21] using techniques derived ffrom the Duffing model.[24,25] We show in Figure 1c the dependence of the maximum amplitude, $a(\omega)$, for a different driving force V_{ac}. When the driving force exceeds a given threshold, the oscillator shows bistability and hysteresis.[14]

Our results are in reasonable agreement with the experimental data[14] shown in the inset. Time varying deformation of graphene modifies its electronic spectrum through the modulation of electrostatic doping and in-plane strain modeled with

$$\mathcal{E}_{dg}(t) = \varepsilon_d\{1 + \delta\varepsilon_d \sin(\omega t)\}^{1/2}$$

$$\mathcal{U}_{xx}(t) = u_{xx}\{1 + \delta u_{xx} \sin(\omega t + \phi)\}^2 - \frac{\Delta L}{L} \quad (2)$$

where $\mathcal{E}_{dg}$ is the Dirac point energy in graphene with Fermi energy taken as zero, and $\varepsilon_d = \hbar v_f(\pi C_T V_{dc}/e)^{1/2}$, $\delta\varepsilon_d = V_{ac}/V_{dc}$, $u_{xx} = 8h_0^2/3L^2$, and $\delta u_{xx} = a/h_0$. The internal parameters, $\mathcal{E}_d$ and $\mathcal{U}_{xx}$, constitute the two parameters for adiabatic quantum pumping in graphene NEMs and are governed by the amplitude and the phase response of the resonator system. Figure 1d,e shows the dependence of amplitude $a(\omega_0)$ and the phase response $\phi(\omega_0)$ on V_{ac} and the quality factor Q. Improvements in quality factor, where values as high as $Q = 10^5$ at T = 90 mK have been reported,[26] will lead to stronger nonlinearity and sensitivity.

Cyclic variation of the two internal parameters given by eq 2 constitutes a scheme for quantum pumping. The scattering wave $\psi_j(x)$ in the various regions: left contact, graphene, and right contact, denoted by the subscript $j = l,g,r$, respectively, can be written as follows:

$$\psi_j(x) = \begin{cases} \begin{pmatrix} 1 \\ \eta_l \end{pmatrix} e^{ik_{xl}x} + \mathcal{R}_v \begin{pmatrix} 1 \\ -\eta_l^\dagger \end{pmatrix} e^{-ik_{xl}x} \\ \alpha_l \begin{pmatrix} 1 \\ \eta_g \end{pmatrix} e^{ik_{xg}x} + \alpha_g \begin{pmatrix} 1 \\ -\eta_g^\dagger \end{pmatrix} e^{-ik_{xg}x} \\ \mathcal{T}_v \sqrt{\dfrac{k_{xl}k_{fr}}{k_{xr}k_{fl}}} \begin{pmatrix} 1 \\ \eta_r \end{pmatrix} e^{ik_{xr}x} \end{cases} \quad (3)$$

Here, η_j is the pseudospin phases defined as, $\eta_j = \hbar v_f((k_{xj} + ik_{yj})/(\mathcal{E}_f - \mathcal{E}_{dj}))$, where $\mathcal{E}_{dj}$ is the Dirac energy in each region. $\mathcal{R}_v$, $\mathcal{T}_v$, α_l, and α_g are the wave amplitude coefficients to be determined by imposing wave continuity at the interfaces. The in-plane strain $\mathcal{U}_{xx}$ leads to an effective gauge potential,[27] $A_y = \pm n_s((\beta\mathcal{U}_{xx}t_c)/(ev_f))$, where $\beta = -(\partial \log(t_c)/\partial \log(b)) \approx 2$, $t_c \approx 3$ eV is the nearest neighbor hopping term, $b \approx 1.4$ Å is the bond length, n_s is a dimensionless geometrical factor which is found numerically to be ≈0.5, and the two signs correspond to the two inequivalent Dirac points in the Brillouin zone, i.e., K and K'. It modifies the transverse wave vector through $\hbar k_{yg} = \hbar k_y - eA_y$. Time varying transport coefficients $\mathcal{R}_v(t)$ and $\mathcal{T}_v(t)$ are determined adiabatically from eq 3. The pumping current for each valley is[20,28]

$$\mathcal{I}_v = i\frac{e\omega}{4\pi^2} \sum_{k_y} \int_0^{2\pi/\omega} dt \int_{-\infty}^{\infty} d\varepsilon \frac{\partial f_0(\varepsilon)}{\partial \varepsilon} \Omega_v(k_y, t) \quad (4)$$

where v denotes the valleys (i.e., K,K'), $f_0(\varepsilon)$ is the Fermi–Dirac distribution, and the pumping coefficient is defined as, $\Omega_v = (\partial\mathcal{T}_v/\partial t)\mathcal{T}_v^\dagger + (\partial\mathcal{R}_v)/\partial t)\mathcal{R}_v^\dagger$ evanescent contributions, albeit small, are also included in the model.

In order for the pumping current to be nonzero, spatial inversion symmetry needs to be broken. Typical charge

dx.doi.org/10.1021/nl2038985 | Nano Lett. 2012, 12, 850–854

pumping scheme employs two electrostatic gates to achieve this.[29] In a NEM-based quantum pump, a number of perturbations will achieve that. In the following, we assume that the left and right contacts are not equivalent, which is modeled by different densities of states. In reality, this can be implemented by using different materials for the two contacts.[30] We assume ballistic transport, which implies that the mean free path, l, is larger than the dimensions of the device, $l \gtrsim L$. This limit can be achieved in clean suspended samples.[16] Diffusive scattering will suppress the effect of the gauge field,[17] so that the modulation of the scattering matrix will be reduced, but for sufficiently low amounts of disorder, a finite pumping current will exist.

Using the model presented above, we consider a prototypical device of L = 50 nm, ΔL = 0 nm, and W = 1 μm. Symmetry of the problem requires that the Hamiltonian $\mathcal{H}_K(k_y) = \mathcal{H}_{K'}(-k_y)$ (y is aligned along the zigzag direction), which also implies $\mathcal{I}_{K,k_y} = \mathcal{I}_{K',-k_y}$. In other words, the pumping current $\mathcal{I}_\upsilon = \Sigma_{k_y}\mathcal{I}_{\upsilon,k_y}$ from valley $\upsilon = K,K'$ must be equal and flow in the same direction. Hence, in a subsequent analysis, we shall consider only one of the valleys, i.e., K. First, we illustrate some of the basic features of electron pumping in graphene NEMs. Figure 2a,b plots the transmission $\mathcal{T}_K(k_y)$ and pumping coefficient $\Omega_K(k_y)$ over a pumping cycle for $\phi = 0$ (top panels) and $\phi = \pi/2$ (bottom panels). In these calculations, we assumed an asymmetric contact doping of $\mathcal{E}_{dl} = -0.4$ eV and $\mathcal{E}_{dr} = -0.3$ eV. The contact with a lower doping will stipulate the maximum allowable transverse momentum wave vector (k_{max}) that could accommodate propagating states through the device. As the graphene resonator undergoes strain modulation, it induces a translation in its transverse momentum $\hbar k_{yg} = \hbar k_y - eA_y$. States where $k_{yg} > k_{max}$ would be evanescent in the contacts and their transport coefficients will be zero, i.e., white regions in Figure 2a,b. In general, larger k_y states lead to stronger interference effects, as seen in Figure 2a. Since pumping current is proportional to the accumulated complex phase per cycle, Ω_K is most significant at larger k_y. When the two parameters are in phase, Ω_K for a given k_y state is exactly antisymmetric within each time cycle, i.e., the $\pi/2 \rightarrow 3\pi/2$ is antisymmetric with $-\pi/2 \rightarrow \pi/2$ portion of the cycle, hence $\mathcal{I}_K = 0$. This symmetry is broken when $\phi \neq 0$, and a finite pump current then ensues.

Figure 2c,d plots the time averaged conductance $\langle G \rangle$ and the pumped charge per cycle Q_c for varying transverse momentum, k_y, and doping, $\mathcal{E}_{dg}$. Here, we observe a larger Ω_K at negative k_y and vice versa for K' valley, i.e., a valley Hall effect. Based on the condition $\mathcal{I}_{K,ky} = I_{K',-ky}$ stated earlier, it is apparent that a valley Hall effect will be present, since $\mathcal{I}_{K,ky} \neq \mathcal{I}_{K,-ky}$ in general. The valley Hall effect will induce a spatially dependent valley polarized current, whose effect is maximal near the two edges. Calculations as shown in Figure 2d estimate the valley polarization, i.e., $(\mathcal{I}_K - \mathcal{I}_{K'})/I_K$, to be as large as 90%. Figure 2e–g shows that the pumped charge Q_c is linear with respect to the amplitudes of the pumping parameters and the device length. The latter is a result of increasing interferences frequency with L. Q_c also increases with contacts doping asymmetry, except that the effect maximizes when density of states in one of the contacts becomes the bottleneck to conduction. Reasonable driving voltages lead to measurable currents for devices with similar features to experimentally studied NEMs. These systems provide a robust setup where quantum pumping can be observed.

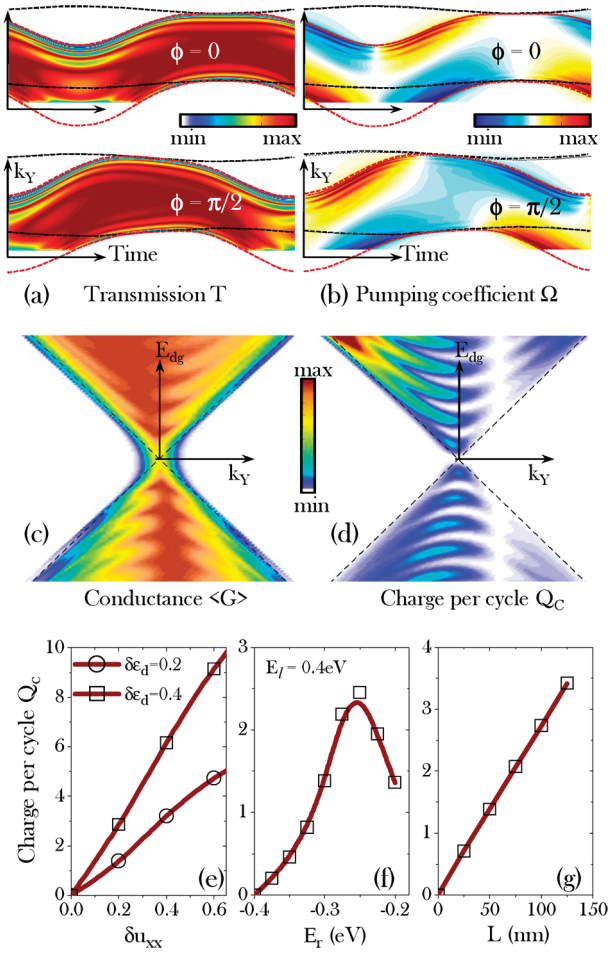

Figure 2. We consider graphene NEM-based electron pumping device through cyclic variations of $\mathcal{E}_d(t)$ and $\mathcal{U}_{xx}(t)$ as described in eq 2. Unless stated otherwise, we consider the graphene dimension of L = 50 nm, ΔL = 0 nm, and W = 1 μm, with equilibrium parameters u_{xx} = 0.02 and $\varepsilon_d = -0.2$ eV. Contact asymmetry is introduced through $\mathcal{E}_{dl} = -0.4$ eV and $\mathcal{E}_{dr} = -0.3$ eV. (a) Transmission, $\mathcal{T}_K(k_y)$, as function of time over one pumping cycle, for cases where the two parametric variations are in-phase (i.e., $\phi = 0$) and out-of-phase (i.e., $\phi = \pi/2$). In these calculations, we assumed $\delta u_{xx} = 0.8$ and $\delta\mathcal{E}_{dg} = 0.2$. Dashed lines indicate the minimum and maximum transverse momentum k_y (black) and $k_y - (e/\hbar)A_y$ (red). (b) Similar to (a), except for pumping coefficient $\Omega_K(k_y)$. Note that pumping current for the $\phi = 0$ case is zero. (c,d) Time-averaged conductance $\langle G \rangle$ and charges per cycle Q_c as function of graphene's doping $\mathcal{E}_{dg}$ and transverse momentum k_y. Dashed lines indicate $\pm \hbar v_f(k_y - (e/\hbar)A_y)$. In these calculations, we assumed $\delta u_{xx} = 0.2$ and $\delta\mathcal{E}_{dg} = 0.2$. Note that calculations for (a–d) are performed for only one of the valley, i.e., K. (e–g) studies Q_c as function of various parameters: pumping amplitude δu_{xx}, contact doping asymmetry, and device length L. In these calculations, we assumed $\delta u_{xx} = 0.2$ and $\delta\mathcal{E}_{dg} = 0.2$, unless stated otherwise.

We briefly discuss issues related to experimental realization. In a conventional quantum pumping scheme, displacement current induced by stray capacitances can interfere with the quantum pumping dc current,[29,31] as the two gates can work in unison to result in a rectification of the displacement currents.[32] Since our proposal utilizes only a single back gate, there will be no rectification of the ac displacement currents at least to the first order in frequency. The calculated values of the current in our device are such that situations where the charge pumping per cycle is close to one or a few electrons are feasible.

dx.doi.org/10.1021/nl2038985 | Nano Lett. 2012, 12, 850–854

Coulomb blockade effects will favor the transference of an integer number of electrons per cycle, so that the ratio between current and frequency will be quantized. Such behavior will manifest itself as steps in the dependence of this ratio on driving voltage. The charging energy of a device of length L is $E_c \approx e^2/L$, so that $E_c \sim 10$ K for $L \sim 1$ μm, and Coulomb blockade effects can be expected to be relevant at lower temperatures. The observation of quantized steps in $\mathcal{I}/\omega$ will allow for the realization of a graphene-based current standard,[33] making graphene an unique material from whom current and resistance[34] standards can be fabricated. Note also that the carrier density in very clean suspended graphene samples can be adjusted with great accuracy, making the physics at the Dirac point accessible.[16] At these concentrations, electronic transport in ballistic systems is determined by evanescent waves,[35,36] and pumping through these modes can also be expected.[37] In principle, we also envision alternative schemes via optical means,[38] where the laser could induce a nonequilibrium electronic temperature which, through coupling with the flexural phonons, will lead to strains and vibrations.

In summary, we show that a graphene NEM near resonance can function as an adiabatic quantum pump under realistic experimental conditions due to the unique electronic coupling to the strains induced by long wavelength vibrations. Experimental realization of this effect would open up new opportunities in fundamental and applied research with graphene NEMs.[1−3]

■ ASSOCIATED CONTENT

Supporting Information

Details on the modeling of graphene mechanical resonator is provided. This material is available free of charge via the Internet at http://pubs.acs.org

■ AUTHOR INFORMATION

Corresponding Author

*E-mail: tonyaslow@gmail.com.

Notes

The authors declare no competing financial interest.

■ ACKNOWLEDGMENTS

We thank P. Avouris, P. Kim, and J. Hone for helpful discussions. T.L. is partially supported by the INDEX program under the Nanoelectronic Research Initiatives. Y.-J.J. acknowledges the support from the National Natural Science Foundation of China (under grant no.11004174) and the program for Innovative Research Team in Zhejiang Normal University. The work of M.I.K. is part of the research program of the Stichting voor Fundamenteel Onderzoek der Materie (FOM), which is financially supported by the Nederlandse Organisatie voor Wetenschappelijk Onderzoek (NWO). F.G. is supported by MICINN through grants FIS2008-00124 and CONSOLIDER CSD2007-00010.

■ REFERENCES

(1) Craighead, H. G. Nanoelectromechanical systems. *Science* **2000**, *250*, 1532.

(2) Blencowe, M. Quantum electromechanical systems. *Phys. Rep.* **2004**, *395*, 159.

(3) Ekinci, K. L.; Roukes, M. L. Nanoelectromechanical systems. *Rev. Sci. Instrum.* **2005**, *76*, 061101.

(4) Geerligs, L. J.; Anderegg, V. F.; Holweg, P. A. M.; Mooij, J. E.; Pothier, H.; Esteve, D.; Urbina, C.; Devoret, M. H. Frequency-locked turnstile device for single electrons. *Phys. Rev. Lett.* **1990**, *64* (22), 2691−2694.

(5) Pothier, H.; Lafarge, P.; Urbina, C.; Esteve, D.; Devoret, M. H. Single-electron pump based on charging effects. *Europhys. Lett.* **1992**, *17*, 249.

(6) Pekola, J. P.; Vartiainen, J. J.; Möttönen, M.; Saira, O.-P.; Meschke, M.; Averin, D. V. Hybrid single-electron transistor as a source of quantized electric current. *Nat. Phys.* **2008**, *4*, 120.

(7) Gorelik, L. Y.; Isacsson, A.; Voinova, M. V.; Kasemo, B.; Shekhter, R. I.; Jonson, M. Shuttle mechanism for charge transfer in coulomb blockade nanostructures. *Phys. Rev. Lett.* **1998**, *80* (no. 20), 4526.

(8) Sazonova, V.; Yaish, Y.; Ustunel, H.; Roundy, D.; Arias, T. A.; McEuen, P. L. A tunable carbon nanotube electromechanical oscillator. *Nature* **2004**, *431*, 284.

(9) Azuma, Y.; Hatanaka, T.; Kanehara, M.; Teranishi, T.; Chorley, S.; Prance, J.; Smit, C. G.; Majima, Y. One by one single-electron transport in nanomechanical coulomb blockade shuttle. *Appl. Phys. Lett.* **2007**, *91*, 053120.

(10) Koenig, D. R.; Weig, E. M.; Kotthaus, J. P. Ultrasonically driven nanomechanical single-electron shuttle. *Nat. Nanotechnol.* **2008**, *3*, 482.

(11) Talyanskii, V. I.; Shilton, J. M.; Pepper, M.; Smith, C. G.; Ford, C. J. B.; Linfield, E. H.; Ritchie, D. A.; Jones, G. A. C. Single-electron transport in a one-dimensional channel by high-frequency surface acoustic waves. *Phys. Rev. B* **1997**, *56*, 15180.

(12) Bunch, J. S.; van der Zande, A. M.; Verbridge, S. S.; Frank, I. W.; Tanenbaum, D. M.; Parpia, J. M.; Craighead, H. G.; McEuen, P. L. Electromechanical resonators from graphene sheets. *Science* **2007**, *315*, 490.

(13) Garcia-Sanchez, D.; van der Zande, A. M.; San Paulo, B. L. A.; McEuen, P. L.; Bachtold, A. Imaging mechanical vibrations in suspended graphene sheets. *Nano Lett.* **2008**, *8*, 1399.

(14) Chen, C.; Rosenblatt, S.; Bolotin, K. I.; Kalb, W.; Kim, P.; Kymissis, I.; Stormer, H. L.; Heinz, T. F.; Hone, J. Performance of monolayer graphene nanomechanical resonators with electrical readout. *Nat. Nanotechnol.* **2009**, *4*, 861.

(15) Bolotin, K. I.; Sikes, K. J.; Jiang, Z.; Fudenberg, G.; Hone, J.; Kim, P.; , Stormer, H. L.; , "Ultrahigh electron mobility in suspended graphene," *Solid State Commun.*, **2008**, *156*, XXX.

(16) Castro, E. V.; Ochoa, H.; Katsnelson, M. I.; Gorbachev, R. V.; Elias, D. C.; Novoselov, K. S.; Geim, A. K.; Guinea, F. Limits on charge carrier mobility in suspended graphene due to flexural phonons. *Phys. Rev. Lett.* **2010**, *105* (26), 266601.

(17) Fogler, M. M.; Guinea, F.; Katsnelson, M. I. Pseudomagnetic fields and ballistic transport in a suspended graphene sheet. *Phys. Rev. Lett.* **2008**, *101* (22), 226804.

(18) Thouless, D. J. Quantization of particle transport. *Phys. Rev. B* **1983**, *27*, 6083.

(19) Niu, Q. Towards a quantum pump of electric charges. *Phys. Rev. Lett.* **1990**, *64*, 1812.

(20) Brouwer, P. W. Scattering approach to parametric pumping. *Phys. Rev. B* **1998**, *58* (16), R10135.

(21) See Supporting Information.

(22) Xu, Y.; Chen, C.; Deshpande, V. V.; DiRenno, F. A.; Gondarenko, A.; Heinz, D. B.; Liu, S.; Kim, P.; Hone, J. Radio frequency electrical transduction of graphene mechanical resonators. *Appl. Phys. Lett.* **2010**, *97*, 243111.

(23) Peng, H. B.; Chang, C. W.; Aloni, S.; Yuzvinsky, T. D.; Zettl, A. Ultrahigh frequency nanotube resonators. *Phys. Rev. Lett.* **2006**, *97*, 087203.

(24) Thomson, W. T.; Dahleh, M. D. *Theory of vibrations with applications*, Prentice Hall: Upper Saddle River, NJ, 1997.

(25) Duffing, G.; Erzwungene schwingungen bei veränderlicher eigenfrequenz und ihre technische bedeutung, *Braunschweig Vieweg*, **1918**.

(26) Eichler, A.; Moser, J.; Chaste, J.; Zdrojek, M.; Rae, I. W.; , Bachtold, A.; , "Nonlinear damping in mechanical resonators based on graphene and carbon nanotubes," arXiv:1103.1788, 2011.

(27) Vozmediano, M. A. H.; Katsnelson, M. I.; Guinea, F. Gauge fields in graphene. *Phys. Rep.* **2010**, *496*, 109.
(28) Moskalets, M.; Büttiker, M. Floquet scattering theory of quantum pumps. *Phys. Rev. B* **2002**, *66* (20), 205320.
(29) Switkes, M.; Marcus, C. M.; Campman, K.; Gossard, A. C. An adiabatic quantum electron pump. *Science* **1999**, *283*, 1905.
(30) Giovannetti, G.; Khomyakov, P. A.; Brocks, G.; Karpan, V. M.; van den Brink, J.; Kelly, P. J. Doping graphene with metal contacts. *Phys. Rev. Lett.* **2008**, *101*, 026803.
(31) DiCarlo, L.; Marcus, C. M.; Harris, S. J. Jr Photocurrent, rectification, and magnetic field symmetry of induced current through quantum dots. *Phys. Rev. Lett.* **2003**, *91*, 246804.
(32) Brouwer, P. W. Rectification of displacement currents in an adiabatic electron pump. *Phys. Rev. B* **2001**, *63*, 121303(R).
(33) Averin, D. V.; Likharev, K. K. In *Mesoscopic phenomena in solids*; Alschuler, B. L., Lee, P. A., Webb, R. A., Eds.; Elsevier: Amsterdam, The Netherlands, 1991; chpt. 6, p 167.
(34) Tzalenchuk, A.; Lara-Avila, S.; Kalaboukhov, A.; Paolillo, S.; Syväjärvi, M.; Yakimova, R.; Kazakova, O.; Janssen, T. J. B. M.; Fal'ko, V.; Kubatkin, S. Towards a quantum resistance standard based on epitaxial graphene. *Nat. Nanotechnol.* **2010**, *5*, 187.
(35) Katsnelson, M. I. Zitterbewegung, chirality, and minimal conductivity in graphene. *Eur. Phys. Journ. B* **2006**, *51*, 157.
(36) Tworzydło, J.; Trauzettel, B.; Titov, M.; Rycerz, A.; Beenakker, C. W. J. Sub-poissonian shot noise in graphene. *Phys. Rev. Lett.* **2006**, *96* (no. 24), 246802.
(37) Prada, E.; San-Jose, P.; Schomerus, H. Quantum pumping in graphene. *Phys. Rev. B* **2009**, *80* (24), 245414.
(38) Ilic, B.; Krylov, S.; Aubin, K.; Reichenbach, R.; Craighead, H. G. Optical excitation of nanoelectromechanical oscillators. *Appl. Phys. Lett.* **2005**, *86*, 193114.